Journal of Alloys and Compounds 815 (2020) 152419

Contents lists available at ScienceDirect

Journal of Alloys and Compounds

journal homepage: http://www.elsevier.com/locate/jalcom

Enhanced age-hardening response in Mg–Zn–Co alloys with Bi additions

C. He [a], C.Q. Liu [a], H.W. Chen [a, b, *], J.F. Nie [a, b, c, **]

[a] International Joint Laboratory for Light Alloys (Ministry of Education), College of Materials Science and Engineering, Chongqing University, Chongqing, 400044, PR China
[b] Electron Microscopy Center, Chongqing University, Chongqing, 400044, PR China
[c] Department of Materials Science and Engineering, Monash University, Victoria, 3800, Australia

ARTICLE INFO

Article history:
Received 10 April 2019
Received in revised form
19 September 2019
Accepted 23 September 2019
Available online 23 September 2019

Keywords:
Magnesium alloys
Age-hardening
Heterogeneous precipitation
Interface segregation

ABSTRACT

Effects of Bi additions on age-hardening response and precipitation of Mg–2.31Zn–0.31Co (at.%) alloy have been investigated. The addition of Bi can substantially promote the age-hardening response at 200 °C. The precipitates microstructure is characterized using high-angle annular dark-field scanning transmission electron microscope, and the results show that the remarkable improvement is attributed to a much higher number density of β_1' rods and the formation of prismatic Mg_3Bi_2 plates. At the early stage of ageing, Mg_3Bi_2 precipitates out first and then Zn segregates to the Mg_3Bi_2/Mg interface, which could provide chemical environment and heterogeneous nucleation sites for the subsequent precipitation of the β_1' phase.

1. Introduction

Due to the potential in developing low-cost and high-strength wrought Mg alloys without rare earth (RE) elements, Mg–Zn–based alloys have received considerable attention in the last decade. These alloys are known as precipitation-hardenable since the equilibrium solid solubility of Zn in Mg is 2.4 at.% (or 6.2 wt%) at 340 °C (eutectic temperature), and decreases substantially with a drop in temperature, to ~1.1 at.% (or 2.9 wt%) at 200 °C [1]. It has been generally accepted that the strengthening precipitate phases in these alloys include β_1' and β_2' [2–7]. The β_1' phase often forms as $[0001]_\alpha$ rods and was previously described as $MgZn_2$ (space group $P6_3/mmc$, $a = 0.5221$ nm, $c = 0.8567$ nm) [8] or Mg_4Zn_7 (space group $C2/m$, $a = 2.596$ nm, $b = 0.524$ nm, $c = 2.678$ nm, $\beta = 148.6°$) [9]. Several other studies also reported that each single β_1' precipitate usually contains different domains and planar defects [6,10–12]. Such defects were confirmed and characterized by the high-angle annular dark-field scanning transmission electron microscopy (HAADF-STEM) with an atomic-resolution in recent reports [13,14]. The β_2' phase often forms as $(0001)_\alpha$ plates even though it has the $MgZn_2$ structure (space group $P6_3/mmc$, $a = 0.5221$ nm, $c = 0.8567$ nm) [10]. In general, the contribution of β_2' to age-hardening response is very limited due to the rather small volume fraction compared with that of β_1'.

However, Mg–Zn binary alloys [2,3] often show a moderate age hardening response, due to the coarse size and the limited number density of rod-like β_1' precipitates. It was reported that small additions of Ca [15], Ag [7], Cu [16] or the combined addition of Ag and Ca [7,17] to the Mg–Zn binary alloys could result in denser distributions of β_1' precipitates in the peak-aged condition, and thus dramatically enhance the age-hardening response. First-principles calculations [18] revealed that all these three elements have favourable binding energies with vacancies, which would affect the solute diffusion kinetics and the later ageing-precipitation process. Actually, Bi also has a large binding energy with vacancies in Mg [18]. It is thus of interest to determine whether Bi additions have the similar effect as Ca, Ag and Cu elements. On the other hand, Bi additions to Mg can form Mg_3Bi_2 precipitates during the ageing process [19,20], and the age-hardening response of Mg–Bi alloys can be further enhanced by the additions of Zn, which was

* Corresponding author. International Joint Laboratory for Light Alloys (Ministry of Education), College of Materials Science and Engineering, Chongqing University, Chongqing, 400044, PR China.
** Corresponding author. International Joint Laboratory for Light Alloys (Ministry of Education), College of Materials Science and Engineering, Chongqing University, Chongqing, 400044, PR China.
E-mail addresses: hwchen@cqu.edu.cn (H.W. Chen), jianfeng.nie@monash.edu (J.F. Nie).

https://doi.org/10.1016/j.jallcom.2019.152419
0925-8388/

attributed to the formation of finer Mg_3Bi_2 plate precipitates on the prismatic plane of magnesium matrix [20]. A hypothesis that Mg_3Bi_2 precipitates might heterogeneously nucleate on β_1' precipitates has been proposed [20] but not yet been experimentally verified.

It is the purpose of this work to report our results on the effects of Bi additions on age-hardening responses and heterogeneous precipitation in Mg–Zn–Co–Bi alloys. It is found that the Bi addition can significantly enhance the age-hardening response, which is attributed to the refined distribution of β_1' and the formation of prismatic Mg_3Bi_2 precipitate plates. Heterogeneous precipitation is found and its origin is studied using aberration-corrected scanning transmission electron microscopy and energy dispersive spectrometry (EDS) mapping.

2. Material and methods

Alloys of nominal composition of Mg–2.31Zn–0.31Co (at.%) with additions of 0, 0.12, 0.25, 0.37 at.% Bi were prepared from high-purity Mg, Zn, Bi and Mg–8.5Co (at.%) master alloy by induction melting in a mild steel crucible under a protective atmosphere of gas mixture (SF_6 + CO_2) and casting into a steel mould. Small additions of Co used here is to enhance the eutectic temperature and thus to permit a higher solution treatment temperature [21]. To avoid local melting during solution treatment, samples embedded in graphite powder were firstly heat treated at 320 °C for 28 h and then the temperature was raised from 320 °C to 450 °C at a ramp rate of 1 °C/min and held for 12 h, followed by water quenching and ageing in an oil bath at 200 °C. Vickers hardness test was carried out using a load of 1 kg. The hardness value was determined from the average of 10 individual indentations in which the maximum and minimum values were abandoned. Thin foil specimens for HAADF-STEM observations were prepared by ion-beam milling using Gatan PIPS 691 at −70 °C. Characterization of precipitate microstructures and EDS mapping were performed using a Cs-corrected FEI Titan G2 60–300 ChemiSTEM, operated at 300 kV and equipped with a Super-X EDS with four windowless silicon-drift detectors. The thickness of TEM foil was determined using the convergent beam electron diffraction pattern under a two-beam condition [22], and its value was used for calculating the number density and volume fraction of precipitates. For the statistic analysis, around 2000 precipitates in four grains of each alloy were counted.

3. Results

Fig. 1 shows the hardness curves of all the alloys during isothermal ageing treatment at 200 °C, and important features related to the age-hardening curves such as the as-quenched hardness, peak hardness, the time to reach peak hardness and hardness increment are listed in Table 1. The hardness values of the as-quenched alloys are nearly the same, ranging from ~48 to 50 HV. Mg–2.31Zn–0.31Co alloy exhibits a moderate age-hardening response, with a peak hardness value of ~68 HV at 5 h. The age-hardening response is improved with the increasing Bi content in alloys. When 0.37 at.% Bi is added to the Mg–2.31Zn–0.31Co alloy, the hardness is enhanced rapidly to a maximum peak hardness value of 78 HV after only 2.5 h. The increment in hardness is about 28 HV, nearly 1.5 times higher than that of Bi-free alloy (19 HV) and the time to reach peak value is also reduced by half. The addition of 0.37 at.% Bi to the Mg–2.31Zn–0.31Co alloy leads to a 47% increase in hardness increment and a 50% reduction in time to reach the peak hardness.

Fig. 2a shows the backscattered electron (BSE) micrograph of solution-treated sample of Mg–2.31Zn–0.31Co–0.37Bi alloy, and intermetallic particles with different contrast are observed.

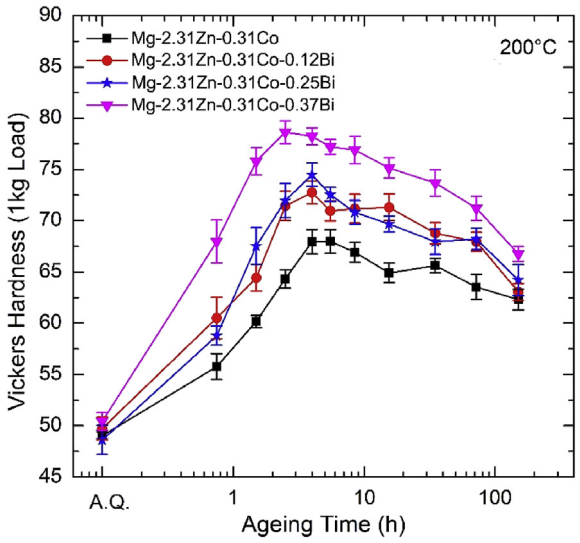

Fig. 1. Age-hardening curves of Mg–2.31Zn–0.31Co–*x*Bi ($x = 0$, 0.12, 0.25 and 0.37) alloys aged isothermally at 200 °C.

Figs. 2b–2d show the corresponding EDS mapping results. According to the EDS mapping results, the intermetallic particles with high and low brightness should be Mg_3Bi_2 [20] and $MgZn_2$ [7], respectively. Co segregation in Mg_3Bi_2 and $MgZn_2$ particles is also observed, as shown in Fig. 2d. It should be noted that Co is not detected in the magnesium matrix in Fig. 2d.

The typical precipitate microstructures in peak-aged samples of Mg–2.31Zn–0.31Co and Mg–2.31Zn–0.31Co–0.37Bi alloys at 200 °C are shown in Fig. 3. The electron beam direction is parallel to (Figs. 3a and 3c) $[0001]_\alpha$ and (Figs. 3b and 3d) $[11\bar{2}0]_\alpha$. In the Bi-free alloy, the microstructure mainly consists of rod-like β_1' precipitates with the long axis parallel to $[0001]_\alpha$, as marked by arrow 1 in Figs. 3a and 3b. The average length and diameter of β_1' rods are ~120 nm and ~16 nm, respectively. These β_1' rods in the α-Mg matrix have a structure of $MgZn_2$ [7] or Mg_4Zn_7 [10] and often contain some domains and planar defects [10,13,14]. In previous studies [7,10], basal β_2' plate precipitates were occasionally observed in peak-aged Mg–Zn binary alloys, but no β_2' precipitates were found in our peak-aged samples. The HAADF-STEM images in Figs. 3c and 3d reveal that there are two kinds of strengthening precipitates in the peak-aged Mg–2.31Zn–0.31Co–0.37Bi alloy, among which the [0001] rods are dominant (marked by arrow 1) and prismatic plates (marked by arrow 2) on $\{11\bar{2}0\}_\alpha$ planes are of a smaller fraction. While the rod-like precipitates are still β_1' phase, they are much finer, Figs. 3c and 3d, ~58 nm in length and ~10 nm in diameter, as shown in Table 2. The number density of rod-like β_1' is 2.6×10^{21} m^{-3}, around 5 times higher than that in the Bi-free alloy, which is comparable to those reported in the peak-aged Mg–3.1Zn–0.25Co alloy at 150 °C [21] and Mg–2.4Zn–0.1Ca–0.1Ag alloy at 160 °C [7]. Those plates lying on $\{11\bar{2}0\}_\alpha$ planes have a near rectangular cross-section when viewed along the $[0001]_\alpha$ direction. The average size is ~43 nm in diameter and ~9 nm in thickness and they have an aspect ratio of ~4.7:1. The number density is about 2.8×10^{20} m^{-3}, Table 2, with the same order of magnitude as β_1' in the Bi-free alloy. These prismatic plate precipitates are actually Mg_3Bi_2 phase and the orientation relationship (OR) between Mg_3Bi_2 precipitate and the matrix is such that $[0001]_{Mg_3Bi_2}//[11\bar{2}0]_{Mg}$ and $(11\bar{2}0)_{Mg_3Bi_2}//(0001)_{Mg}$, which is consistent with a previous study [20]. In addition, [0001] β_1' rods are frequently observed to contact with the prismatic Mg_3Bi_2 plates, as reported previously [20]. A typical example that a β_1' rod

Table 1
Hardness test results of Mg−2.31Zn−0.31Co alloys with and without Bi additions.

Alloy	As-quenched hardness (HV)	Peak hardness (HV)	Time to reach peak hardness (h)	Hardness increment (HV)
Mg−2.31Zn−0.31Co	49	68	5.0	19
Mg−2.31Zn−0.31Co-0.12Bi	49	73	4.0	24
Mg−2.31Zn−0.31Co-0.25Bi	48	74	4.0	26
Mg−2.31Zn−0.31Co-0.37Bi	50	78	2.5	28

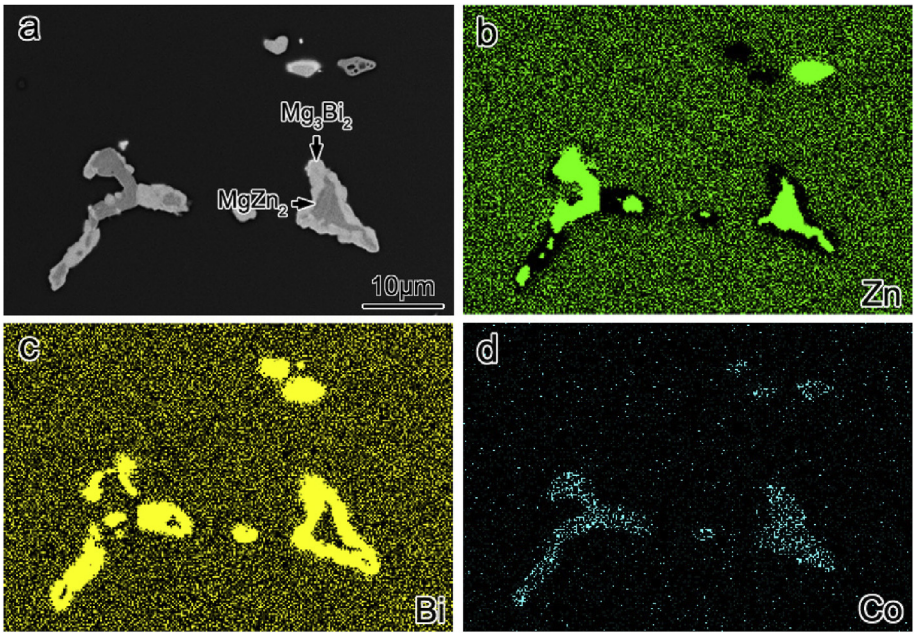

Fig. 2. EDS mapping analysis of retained intermetallic particles in the solution treated Mg−2.31Zn−0.37Bi−0.31Co (at.%) alloy, (a) BSE image, (b) Zn map, (c) Bi map, and (d) Co map.

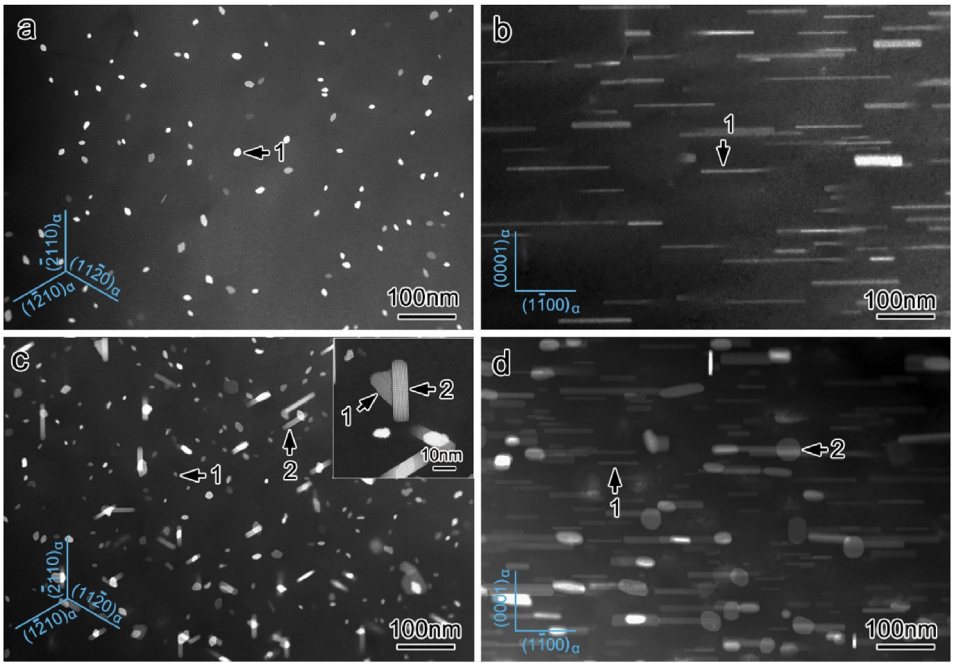

Fig. 3. HAADF-STEM micrographs showing precipitate distributions in peak-aged samples of (a, b) Mg−2.31Zn−0.31Co and (c, d) Mg−2.31Zn−0.31Co−0.37Bi alloys at 200 °C. The electron beam is parallel to (a, b) $[0001]_\alpha$ and (c, d) $[11\bar{2}0]_\alpha$. The rod-like β_1' and prismatic Mg_3Bi_2 precipitates are marked with arrows 1 and 2, respectively.

Table 2
Quantitative microstructural measurements of precipitates in peak-aged samples.

Precipitates	Precipitate size (nm)			Number density	Volume fraction
	Length	Diameter	Thickness	(m^{-3})	(%)
β_1' in Bi-free alloy	120 ± 28	16 ± 5	–	5.1×10^{20}	1.1
β_1' in alloy with 0.37 at.% Bi	58 ± 23	10 ± 4	–	2.6×10^{21}	1.2
Mg_3Bi_2 in alloy with 0.37 at.% Bi	–	43 ± 8	9 ± 3	2.8×10^{20}	0.6

is associated with the broad facet of a Mg_3Bi_2 plate is shown in the upper right inset in Fig. 3c. Large angle tilting suggests that it does not result from an overlapping effect. It is inferred that these two particles precipitate simultaneously or one particle heterogeneously nucleates on the other in Mg–2.31Zn–0.31Co–0.37Bi alloy during the ageing process.

In order to determine whether the heterogeneous precipitation does exist or not, the under-aged microstructure of the Mg–2.31Zn–0.31Co–0.37Bi alloy aged at 200 °C for 0.5 h is also characterized using HAADF-STEM imaging. In the low-magnification HAADF-STEM image shown in Fig. 4, three Mg_3Bi_2 particles are observed. One of them is individually distributed and the other two are coupled with β_1' precipitates of a smaller size. Fig. 5a shows the atomic-resolution HAADF-STEM of an individual Mg_3Bi_2 precipitate shown in Fig. 4, with a small size of ~8 nm in diameter and ~6 nm in thickness. The OR between the Mg_3Bi_2 precipitate and matrix is $[0001]_{Mg_3Bi_2}//[11\bar{2}0]_{Mg}$ and $(11\bar{2}0)_{Mg_3Bi_2}//(0001)_{Mg}$, same with that in the peak-aged samples. There are no other precipitates observed at its periphery of this individual Mg_3Bi_2 precipitate. However, a very small β_1', less than 2 nm in diameter, is observed to have nucleated at the broad facet of another Mg_3Bi_2 particle at the same stage of ageing, as shown in Fig. 5b. A larger β_1' rod that is adhesive to the broad facet of a Mg_3Bi_2 precipitate is also found in Fig. 5c. Thus, it is reasonable to conclude that heterogeneous precipitation indeed occurs, where Mg_3Bi_2 precipitates form first and then serve as heterogeneous sites for β_1'. In addition, it is also observed that some β_1' rods even precipitate at the end (Fig. 6a), corner (Fig. 6b), or two facets (Figs. 6c and 6d) of Mg_3Bi_2 precipitates.

To answer the question why β_1' rods prefer to heterogeneously precipitate at the interfaces of Mg_3Bi_2 plates, EDS mapping is used to characterize these Mg_3Bi_2 precipitates and distribution of Zn. The $[0001]_\alpha$ HAADF-STEM image of a single Mg_3Bi_2 precipitate in an under-aged specimen of the alloy containing 0.37 at.% Bi is shown in Fig. 7a. It has a diameter of ~12 nm and a thickness of ~6 nm. Its OR is same as that in Fig. 5. EDS maps in Figs. 7b and 7c indicate that Zn atoms unambiguously segregate at Mg/Mg_3Bi_2 interfaces at the early stage of ageing. Note that Zn segregation is much more obvious in the broad facets than that in the end facets. This may be due to the fact that the end facets are not in an edge-on orientation. Zn interfacial segregation is further confirmed when EDS mapping is performed along $[1\bar{1}00]_\alpha$, as shown in Figs. 7e and 7f. Such interfacial segregation of solute atoms is similar to Nd segregation at Mg/Zn_2Zr_3 interfaces [23], Zn at Mg/Mg_2Sn interfaces [24], Ag at $Mg/Mg_{17}Al_{12}$ interfaces [25] and Zn at $Mg/Mg_{17}Al_{12}$ interfaces [26].

With the prolonging of ageing time, Zn segregation is retained in peak-aged samples of the Mg–2.31Zn–0.31Co–0.37Bi alloy. Fig. 8a and 8d shows HAADF-STEM images of Mg_3Bi_2 plates coupled with β_1' rods at the board facet and end facet in a peak-aged sample, respectively. The corresponding EDS maps in Figs. 8b–c and 8e–8f reveal the obvious segregation of Zn atoms in the interfaces between Mg_3Bi_2 and magnesium matrix.

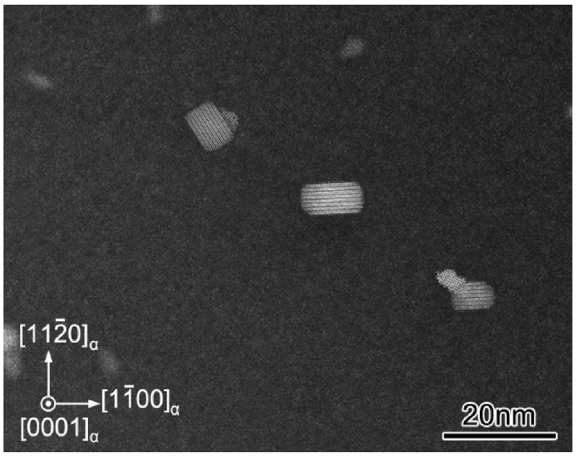

Fig. 4. Low-magnification HAADF-STEM micrograph showing the microstructure of Mg–2.31Zn–0.31Co–0.37Bi alloy aged at 200 °C for 0.5 h. The electron beam is parallel to $[0001]_\alpha$.

4. Discussion

The addition of 0.37 at.% Bi to the Mg–2.31Zn–0.31Co alloy improves the age-hardening response, Fig. 1, which can be ascribed to a much higher number density of β_1' rods in peak-aged samples and the precipitation of prismatic Mg_3Bi_2 plates in the α-Mg matrix. First-principles calculations [18] reveal that Bi has a quite large binding energy with vacancies in Mg, which suggests that more vacancies might be trapped by Bi atoms in the α-Mg matrix rather than annihilate at grain boundaries after the solution heat treatment. During the ageing process, the diffusion rate of Zn atoms is expected to be remarkably enhanced, thus resulting in the formation of more supercritical nucleus of β_1', according to the classical nucleation theory on solid-state phase transformations [27]. This indicates that a higher homogeneous nucleation rate of β_1' in Mg–2.31Zn–0.31Co–0.37Bi alloy is expected during the ageing at 200 °C.

In addition, Co fully segregates into to the retained Mg_3Bi_2 and $MgZn_2$ intermetallic particles after solution treatment of Mg–2.31Zn–0.31Co–0.37Bi alloy, and it is not detected in the matrix, as shown in Fig. 2d, which is consistent with that reported in Mg–8Zn–0.6Co (wt%) alloy. Therefore, the effect of Co on Mg solid solution decomposition could be neglected.

It should be noted that nearly all Mg_3Bi_2 precipitates contact with a rod-like β_1' particle in the peak-aged microstructure (Fig. 3). Besides, as clearly revealed in Figs. 4 and 5, the prismatic Mg_3Bi_2 precipitates act as heterogeneous nucleation sites for β_1' phase. Heterogeneous precipitation in Mg alloys has been extensively reported [17,20,28–33], and often occurs at defects, such as dislocations, twin boundaries, interphase boundaries, and grain boundaries. Two main explanations are proposed to rationalize this phenomenon. One is relaxation of strain fields of precipitate. For example, the formation of coupled β_1/β particles in Mg–RE alloys results in self-accommodation of shear strains involved their phase

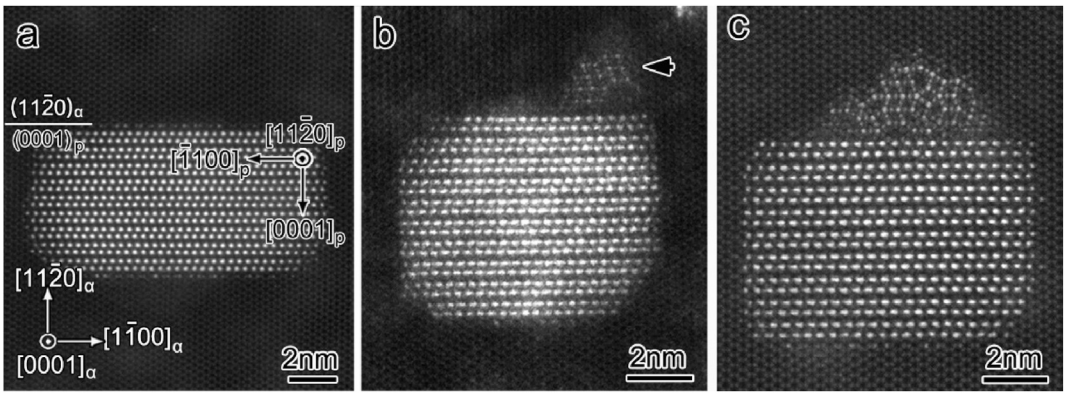

Fig. 5. (a) $[0001]_\alpha$ HAADF-STEM micrograph of an individual Mg_3Bi_2 precipitate. (b and c) $[0001]_\alpha$ HAADF-STEM micrographs showing heterogeneous precipitation of β_1' on broad facets of Mg_3Bi_2 phase. These micrographs are recorded from samples of Mg–2.31Zn–0.31Co–0.37Bi alloy aged at 200 °C for 0.5 h.

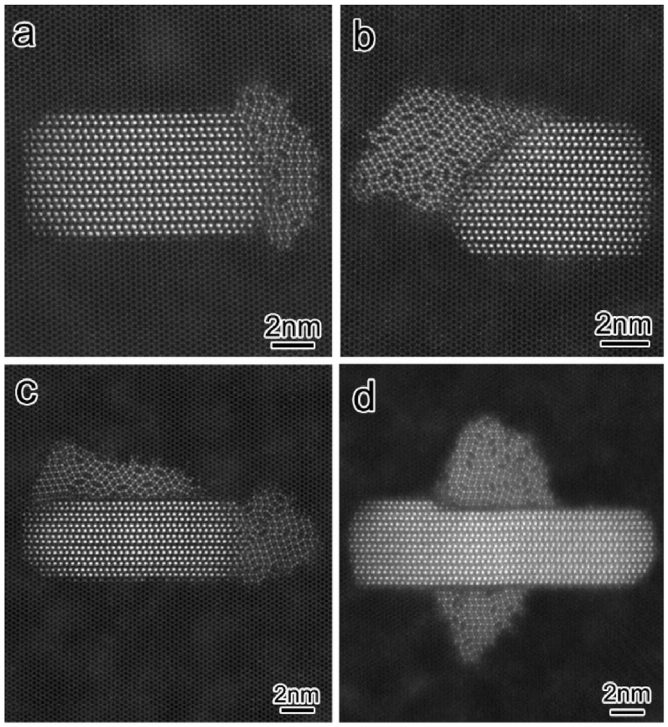

Fig. 6. $[0001]_\alpha$ HAADF-STEM micrographs showing heterogeneous precipitation of β_1' on (a) end, (b) corner and (c, d) two facets of Mg_3Bi_2 phase, recorded from samples of Mg–2.31Zn–0.31Co–0.37Bi alloy aged at 200 °C for 0.5 h.

transformation processes, leading to the common observation of a β_1 invariably attached to β' ends [31]. The other one is that the segregation of solute atoms at defects subsequently promotes the formation of precipitates rich in that solute. It has been reported that segregation of Zn and Al at grain boundaries would act as a precursor for the initiation of the discontinuous precipitation of $Mg_{17}Al_{12}$ in an extruded Mg–8.8Al–1.3Sn–1.2Zn alloy [29] and that Sn–Na clusters provide heterogeneous sites for Mg_2Sn particles in the Mg–2.3Sn–3Al–0.4Zn–0.1Na alloy [32]. In this work, since β_1' rods are observed to form at broad-, end- and even corner-facets of Mg_3Bi_2 precipitates, the heterogeneous precipitation of the β_1' rods does not seem to be related to the detailed structure of the Mg/Mg_3Bi_2 interfaces, Figs. 5 and 6, i.e., it may not be associated with the elastic strain at the interface. Given that Zn atoms segregate to nearly all boundaries of a Mg_3Bi_2 precipitate, Fig. 7, the heterogeneous precipitation is most likely to be caused by the local enrichment of Zn, since the region with Zn segregation provides a chemical environment to transform that region into a Zn-rich β_1' rod.

Therefore, synergic effects of the promoted homogeneous nucleation rate from the higher diffusion rate and heterogeneous nucleation at Mg/Mg_3Bi_2 interfaces (Figs. 3c and 5) will lead to a denser distribution β_1' rods in peak-aged samples than that in the Bi-free alloy, Table 2. Simultaneously, Zn segregation at the Mg/Mg_3Bi_2 interface (Fig. 7) may reduce the interfacial energy, thus decrease the activation energy barrier to homogeneous nucleation, enhancing the nucleation rate and slowing down the coarsening rate of Mg_3Bi_2 phase. This would result in a denser distribution of Mg_3Bi_2 precipitates in the 0.37 at.% Bi-containing alloy, Figs. 3c and 3d. According to a previous work [34], the contribution of $[0001]_\alpha$ rods to the critical resolved shear stress (CRSS) increment due to Orowan strengthening is given as:

$$\Delta\tau = \frac{Gb}{2\pi\sqrt{1-\nu}\left(\frac{0.935}{\sqrt{f}}-1\right)d_t} ln\frac{d_t}{b}, \quad (1)$$

where $\Delta\tau$ is the increment in CRSS, G the shear modulus, b the magnitude of the Burgers vector of slip dislocations, ν the Poisson's ratio, f the volume fraction of precipitates, and d_t the diameter of $[0001]_\alpha$ rods. The increment in CRSS contributed by the prismatic plates can be expressed as:

$$\Delta\tau = \frac{Gb}{2\pi\sqrt{1-\nu}\left(0.825\sqrt{\frac{d_t t_t}{f}}-0.393d_t-0.886t_t\right)} ln\frac{0.886\sqrt{d_t t_t}}{b}, \quad (2)$$

where d_t and t_t are the diameter and thickness of precipitate plates, respectively. In the present case, G, b and ν are constant. The volume fraction (f) and the average sizes (d_t and t_t) were obtained by quantitative microstructural measurements, as shown in Table 2. Thus, the ratio of $\Delta\tau_{(rod)}/\Delta\tau_{(plate)}$ is calculated to be 2.15. It indicates that prismatic Mg_3Bi_2 plates contribute nearly 1/3 to the CRSS increment of Mg–2.31Zn–0.31Co–0.37Bi alloy, though its number density is about 1/10 of that of β_1' rods.

5. Conclusions

The age-hardening response of Mg–2.31Zn–0.31Co alloy at

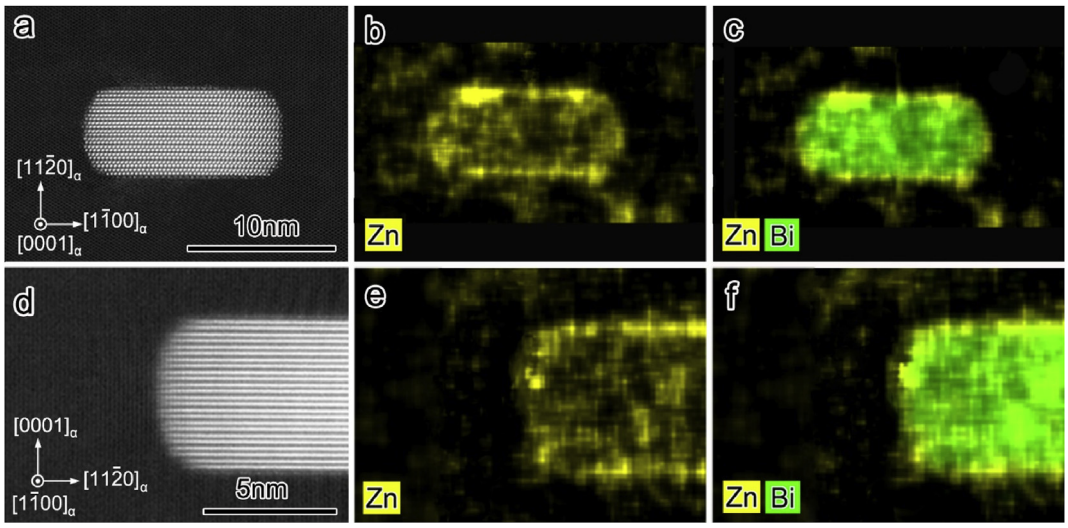

Fig. 7. (a, d) HAADF-STEM micrographs and (b, c, e and f) corresponding EDS maps showing individual Mg_3Bi_2 precipitates in a sample of Mg−2.31Zn−0.31Co−0.37Bi alloy aged at 200 °C for 0.5 h along (a–c) $[0001]_\alpha$ and (d–f) $[1\bar{1}00]_\alpha$, (b, e) Zn maps, (d, f) Bi−Zn composite maps.

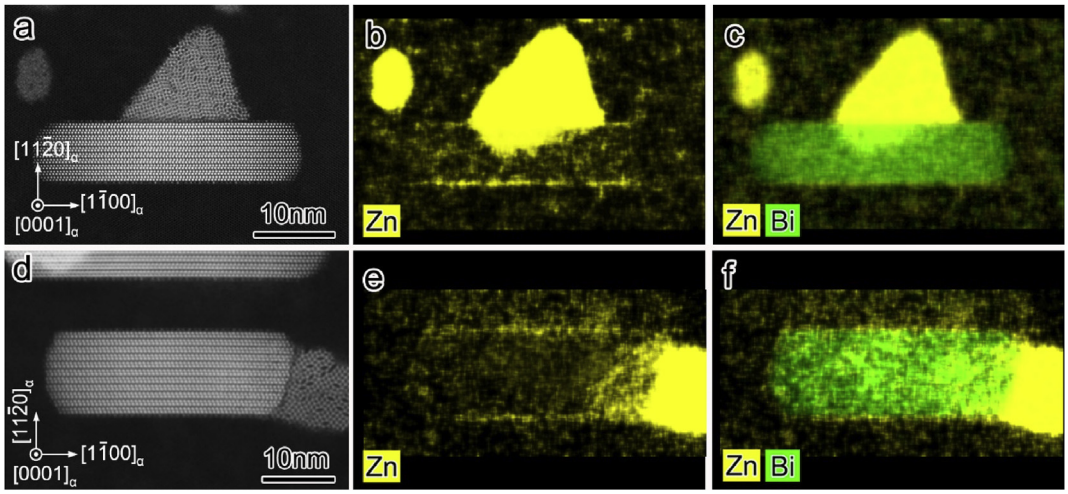

Fig. 8. (a, d) HAADF-STEM micrographs showing rod-like β_1' precipitates attached to the (a) broad facet and (d) end facet of Mg_3Bi_2 precipitates in the peak-aged Mg−2.31Zn−0.31Co−0.37Bi alloy. (b, c, e and f) Corresponding EDS maps of precipitates in (a, d), (b, e) Zn maps, (c, f) Bi−Zn composite maps.

200 °C can be dramatically enhanced by Bi additions. The addition of 0.37 at.% Bi to the Bi-free alloy results in a 47% increase in hardness increment and a 50% reduction in time to reach peak hardness. The significant improvement in precipitation hardening is associated with a higher number density of β_1' rods and the dispersion of prismatic Mg_3Bi_2 plates. Zn atoms segregate to the Mg_3Bi_2/Mg interface at the early stage of ageing and these Zn-rich regions provide heterogeneous nucleation sites for β_1' during continued ageing.

Acknowledgements

This work is supported by National Natural Science Foundation of China (51771036, 51131009 and 51421001), National Key Research and Development Program of China (2016YFB0700402), and Graduate Research and Innovation Foundation of Chongqing, China (Grant No. CYB17004) and the Australian Research Council. The authors are also grateful to the access to the facilities of the Electron Microscopy Center in Chongqing University.

References

[1] A.A. Nayeb-Hashemi, J.B. Clark, Phase Diagrams of Binary Magnesium Alloys, ASM International, Metals Park, OH, 1988.
[2] E.O. Hall, The age-hardening characteristics of two magnesium-zinc alloys, J. Inst. Met. 96 (1968) 21–27.
[3] G. Mima, Y. Tanaka, The aging characteristics of magnesium–4wt% zinc alloy, Trans. Jpn. Inst. Met. 12 (1971) 71–75.
[4] J. Buha, Characterisation of precipitates in an aged Mg–Zn–Ti alloy, J. Alloy. Comp. 472 (2009) 171–177.
[5] F. Qi, D. Zhang, X. Zhang, X. Xu, Effect of Sn addition on the microstructure and mechanical properties of Mg–6Zn–1Mn (wt.%) alloy, J. Alloy. Comp. 585 (2014) 656–666.
[6] J. Jiang, S. Ni, H. Yan, Q. Wu, M. Song, New orientations between β_2' phase and α matrix in a Mg–Zn–Mn alloy processed by high strain rate rolling, J. Alloy. Comp. 750 (2018) 465–470.
[7] C.L. Mendis, K. Oh-ishi, K. Hono, Enhanced age hardening in a Mg–2.4at.% Zn alloy by trace additions of Ag and Ca, Scr. Mater. 57 (2007) 485–488.
[8] Y. Komura, K. Tokunaga, Structural studies of stacking variants in Mg-base Friauf-Laves phases, Acta Crystallogr. 36 (1980) 1548–1554.
[9] Y.P. Yarmolyuk, P.I. Kripyakevich, E.V. Mel'nik, Crystal structure of the compound Mg_4Zn_7, Sov. Phys. Crystallogr. 20 (1975) 329–331.
[10] X. Gao, J.F. Nie, Characterization of strengthening precipitate phases in a Mg–Zn alloy, Scr. Mater. 56 (2007) 645–648.
[11] A. Singh, A.P. Tsai, Structural characteristics of β_1' precipitates in Mg–Zn-based

alloys, Scr. Mater. 57 (2007) 941–944.
[12] J.M. Rosalie, H. Somekawa, A. Singh, T. Mukai, Orientation relationships between icosahedral clusters in hexagonal $MgZn_2$ and monoclinic Mg_4Zn_7 phases in Mg–Zn(–Y) alloys, Philos. Mag. 91 (2011) 2634–2644.
[13] Z. Yang, L. Zhang, M.F. Chisholm, X. Zhou, H. Ye, S.J. Pennycook, Precipitation of binary quasicrystals along dislocations, Nat. Commun. 9 (2018) 809.
[14] H. Xie, H. Pan, Y. Ren, S. Sun, L. Wang, H. Zhao, B. Liu, S. Li, G. Qin, Self-assembly of two unit cells into a nanodomain structure containing five-fold symmetry, J. Phys. Chem. Lett. 9 (2018) 4373–4378.
[15] C.J. Bettles, M.A. Gibson, K. Venkatesan, Enhanced age-hardening behaviour in Mg–4 wt.% Zn micro-alloyed with Ca, Scr. Mater. 51 (2004) 193–197.
[16] J. Buha, T. Ohkubo, Natural aging in Mg–Zn(–Cu) alloys, Met. Mater. Trans. A 39 (2008) 2259–2273.
[17] T. Bhattacharjee, C.L. Mendis, K. Oh-ishi, T. Ohkubo, K. Hono, The effect of Ag and Ca additions on the age hardening response of Mg–Zn alloys, Mater. Sci. Eng. A 575 (2013) 231–240.
[18] D. Shin, C. Wolverton, First-principles study of solute–vacancy binding in magnesium, Acta Mater. 58 (2010) 531–540.
[19] Y.H. Sun, B.Z. Sun, Investigation of structure, morphology and orientation of precipitates in Mg–Bi alloy, Mater. Char. 140 (2018) 129–133.
[20] T.T. Sasaki, T. Ohkubo, K. Hono, Precipitation hardenable Mg–Bi–Zn alloys with prismatic plate precipitates, Scr. Mater. 61 (2009) 72–75.
[21] J. Geng, X. Gao, X.Y. Fang, J.F. Nie, Enhanced age-hardening response of Mg–Zn alloys via Co additions, Scr. Mater. 64 (2011) 506–509.
[22] P. Kelly, A. Jostsons, R. Blake, J. Napier, The determination of foil thickness by scanning transmission electron microscopy, Phys. Status Solidi A 31 (1975) 771–780.
[23] D. Rossouw, B. Langelier, A. Scullion, M. Danaie, G.A. Botton, Multivariate-aided mapping of rare-earth partitioning in a wrought magnesium alloy, Scr. Mater. 124 (2016) 174–178.
[24] C.Q. Liu, H.W. Chen, J.F. Nie, Interphase boundary segregation of Zn in Mg–Sn–Zn alloys, Scr. Mater. 123 (2016) 5–8.
[25] J. Miao, W. Sun, A.D. Klarner, A.A. Luo, Interphase boundary segregation of silver and enhanced precipitation of $Mg_{17}Al_{12}$ Phase in a Mg–Al–Sn–Ag alloy, Scr. Mater. 154 (2018) 192–196.
[26] C.Q. Liu, H.W. Chen, N.C. Wilson, J.F. Nie, Zn segregation in interface between $Mg_{17}Al_{12}$ precipitate and Mg matrix in Mg–Al–Zn alloys, Scr. Mater. 163 (2019) 91–95.
[27] D.A. Porter, K.E. Easterling, M. Shrief, Phase Transformations in Metals and Alloys, (Revised Reprint), CRC Press, Boca Raton, 2009.
[28] T. Honma, T. Ohkubo, S. Kamado, K. Hono, Effect of Zn additions on the age-hardening of Mg–2.0Gd–1.2Y–0.2Zr alloys, Acta Mater. 55 (2007) 4137–4150.
[29] C.Q. Liu, C.L. Liu, H.W. Chen, J.F. Nie, Heat-treatable Mg–9Al–6Sn–3Zn extrusion alloy, J. Mater. Sci. Technol. 34 (2018) 284–290.
[30] Y.M. Zhu, H. Liu, Z. Xu, Y. Wang, J.F. Nie, Linear-chain configuration of precipitates in Mg–Nd alloys, Acta Mater. 83 (2015) 239–247.
[31] Z. Xu, M. Weyland, J.F. Nie, Shear transformation of coupled β_1/β' precipitates in Mg–RE alloys: a quantitative study by aberration corrected STEM, Acta Mater. 81 (2014) 58–70.
[32] F.R. Elsayed, T.T. Sasaki, C.L. Mendis, T. Ohkubo, K. Hono, Significant enhancement of the age-hardening response in Mg–10Sn–3Al–1Zn alloy by Na microalloying, Scr. Mater. 68 (2013) 797–800.
[33] T.T. Sasaki, K. Oh-ishi, T. Ohkubo, K. Hono, Effect of double aging and micro-alloying on the age hardening behavior of a Mg–Sn–Zn alloy, Mater. Sci. Eng. A 530 (2011) 1–8.
[34] J.F. Nie, Effects of precipitate shape and orientation on dispersion strengthening in magnesium alloys, Scr. Mater. 48 (2003) 1009–1015.